PAPER • OPEN ACCESS

A new look on the two-dimensional Ising model: thermal artificial spins

View the article online for updates and enhancements.

New Journal of Physics

The open access journal at the forefront of physics

CrossMark

PAPER

A new look on the two-dimensional Ising model: thermal artificial spins

Unnar B Arnalds[1], Jonathan Chico[2], Henry Stopfel[2], Vassilios Kapaklis[2], Oliver Bärenbold[2], Marc A Verschuuren[3], Ulrike Wolff[4], Volker Neu[4], Anders Bergman[2] and Björgvin Hjörvarsson[2]

1 Science Institute, University of Iceland, Dunhaga 3, IS-107 Reykjavik, Iceland
2 Department of Physics and Astronomy, Uppsala University, SE-75120 Uppsala, Sweden
3 Philips Research Laboratories, Eindhoven, The Netherlands
4 IFW Dresden, Institute of Metallic Materials, D-01171 Dresden, Germany

E-mail: uarnalds@hi.is

Abstract

We present a direct experimental investigation of the thermal ordering in an artificial analogue of an asymmetric two-dimensional Ising system composed of a rectangular array of nano-fabricated magnetostatically interacting islands. During fabrication and below a critical thickness of the magnetic material the islands are thermally fluctuating and thus the system is able to explore its phase space. Above the critical thickness the islands freeze-in resulting in an arrested thermalized state for the array. Determining the magnetic state we demonstrate a genuine artificial two-dimensional Ising system which can be analyzed in the context of nearest neighbor interactions.

The Ising model invented by Wilhelm Lenz and solved in one-dimension by Ernst Ising in 1924 is one of the pillars of statistical mechanics [1, 2]. Although built on a simple basis, that of an interacting system composed of a chain of entities with only two discrete states, $\mathbf{s} = \{1, -1\}$, the Ising model still to this day is used to model magnetic systems and can be applied to a wealth of atomistic and mesoscopic experimental systems ranging from ferromagnetic ordering and atomic-scale antiferromagnets [3] to the ordering of binary colloidal structures [4] and thermal artificial spin systems [5]. In the two-dimensional case spins are arranged on a square lattice and each spin interacts with four nearest neighbors, as seen in figure 1. The total energy of such a two-dimensional Ising system can be described by the equation

$$E = -J_h \sum_{i,j}^{h} \mathbf{s}_i \cdot \mathbf{s}_j - J_v \sum_{i,j}^{v} \mathbf{s}_i \cdot \mathbf{s}_j, \tag{1}$$

where J_h and J_v correspond to interaction energies in the horizontal [10] and vertical [01] lattice directions of the two-dimensional crystal and the sum is taken over all pairs of nearest neighbor spins $\mathbf{s}_i$ and $\mathbf{s}_j$. As opposed to the one-dimensional model which shows no spontaneous magnetization at temperatures $T > 0$ K a spontaneous magnetization appears in the two-dimensional case [6] with an order parameter given by [7, 8]

$$M(T) = \left(1 - \left[\sinh\left(\frac{2J_h}{k_B T} \right) \sinh\left(\frac{2J_v}{k_B T} \right) \right]^{-2} \right)^{\frac{1}{8}}, \tag{2}$$

where T corresponds to the temperature and k_B is the Boltzmann constant. The model is not complicated by the choice of different values or signs of J_h and J_v [7].

Nano-patterned single-domain magnetic thin film islands have been a prominent candidate in recent years for creating artificial analogues of interacting systems. Using modern lithographic techniques it has become feasible to design directly the shape of such islands and their geometrical arrangement creating two-dimensional arrays of interacting artificial spins. Artificial Ising-like spins can be realized by designing elongated islands of thin films materials, for which shape anisotropy confines the magnetization to only two possible orientations. By
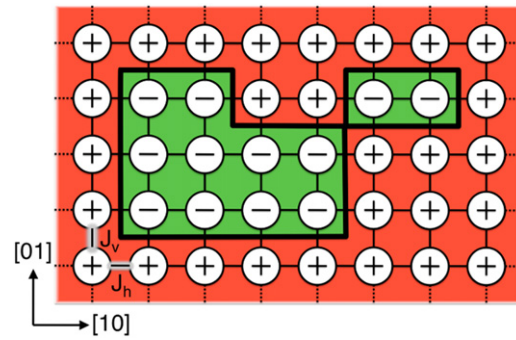
Figure 1. The two-dimensional Ising system. A two-dimensional Ising system consists of an array of spins which are only capable of pointing in two opposite directions, $\mathbf{s} = \pm 1$ and interacting with their four nearest neighbors with interaction energies J_h and J_v along the [10] and [01] lattice directions. At $T = 0$ K the ground state is doubly degenerate consisting of all spins pointing in the $(+)$ or the $(-)$ directions for the case of a symmetric Ising system. For $T > 0$ K defects above the ground state occur enclosed by a domain wall separating the areas of spins in the all $(+)$ or all $(-)$ directions.
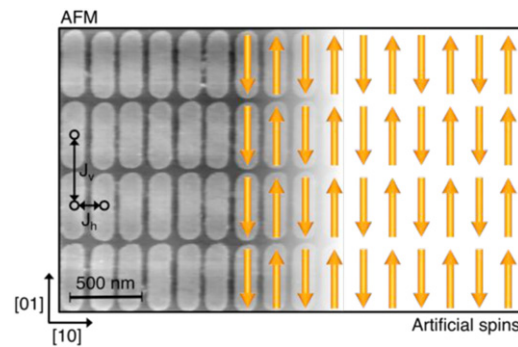

Figure 2. Nano-patterned artificial spins. Atomic force microscopy (AFM) image of part of the patterned array showing the structure and arrangement of the nano-patterned islands (see further information in supplementary material). The shape of the islands confines the magnetization to point along the long axis of the islands and during thermalization at the onset of a frozen state they can be considered as thermally active superspins. In the superspin model the vertical coupling ([01] direction) prefers a ferromagnetic alignment of the spins ($J_v > 0$) whereas the lateral coupling ([10] direction) prefers an antiferromagnetic alignment ($J_h < 0$) resulting in the ground state ordering of the artificial spins illustrated to the right in the figure.

arranging such islands in different geometries a wealth of interacting systems can be studied including cellular automata [9, 10] and frustrated systems such as artificial spin ice with in plane [11–13] and perpendicular realizations [14]. The two-dimensional nano-scale nature of these systems enables their state to be directly determined by imaging techniques such as magnetic force microscopy (MFM) [11, 15], photoemission electron microscopy [16–18] and Lorentz microscopy [19].

In this paper we investigate a two-dimensional array composed of elongated thin film islands in a square lattice (see figure 2). During fabrication the array goes through a dynamic phase enabling the system to thermally explore its phase space leading to a low energy ordered state [15]. After this dynamic phase the state of the system becomes frozen-in, generating a snapshot of an arrested thermalized state. The determination of the magnetization of individual islands in the array allows us to demonstrate that the dynamic phase leads to an ordering of the magnetic state of the array, which can be described by the two-dimensional Ising model.

The thickness regime wherein thermal dynamics of the spins are obtained occurs during the deposition of the magnetic material onto prepatterned substrates as shown by Morgan *et al* [15, 20]. During the deposition, the island thickness (and thereby their volume) becomes gradually larger and the magnetization reversal energy barrier, E_r, associated with their shape anisotropy increases. In the initial stages of the island growth this barrier is smaller than the thermal energy enabling the magnetization to spontaneously fluctuate between the two low energy states defined by the shape anisotropy. As the thickness becomes larger the reversal energy increases, eventually overcoming the thermal energy, reaching a threshold where the superparamagnetic behavior is suppressed as the scale of the combined shape anisotropy reversal energy barrier and the energy landscape of the array are sufficient to lock the magnetization in each of the islands (see figure 3). Subsequently the array can be imaged by MFM and the magnetization direction of each island can be determined (see figure 4).
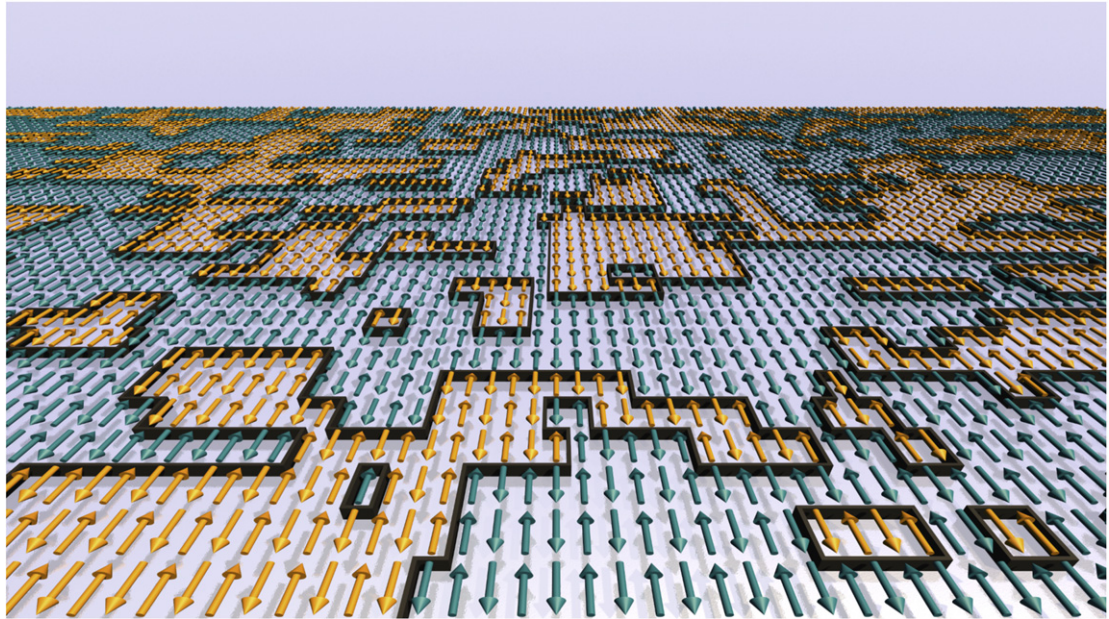
Figure 3. Snapshot of an arrested state. The ordering of the investigated array illustrated through highlighting the twofold degenerate ground state and the domain walls separating them. As compared to a fully ferromagnetic two-dimensional Ising system the antiferromagnetic coupling leads to an additional asymmetry in the population of the up and down islands themselves, which is indicative of the influence of an external field. Out of the $N = 10487$ islands analyzed $n_u = 5294$ were found to point in the up direction while $n_d = 5193$ were found to point in the down direction resulting in an asymmetry within statistical limits. An overview of the entire investigated array as well as a data file containing the directions of all islands is supplied in supplementary material.

During the limited time window where fluctuations occur the fast dynamics allow the array to explore its phase space and achieve an equilibrium condition. During this dynamic phase, before the magnetization becomes frozen, the reversal energy barrier and the interaction energies between neighboring islands are of the order of the thermal energy $k_B T$. For the island sizes and array parameters used for this study the energy values involved correspond to room temperature values for film thicknesses in the ~1 nm regime. Uniform thermal dynamics over the entire array therefore require a well defined, stable thickness of each island in order to minimize randomization effects due to variations in the island thickness and film roughness. Amorphous magnetic materials display soft magnetic properties and a high degree of structural uniformity and are thereby suitable for well defined layers below 1 nm in thickness [21]. For this study we therefore choose amorphous $Co_{68}Fe_{24}Zr_8$ as the island material previously used for creating ultra-thin magnetic layers [22] and well defined nano-patterned multilayered structures [23]. Furthermore, a field imprinted anisotropy can be induced in $Co_{68}Fe_{24}Zr_8$ enhancing the energy barrier for reversal as the magnetization has settled in a fixed direction [24].

Considering magnetostatic interactions in the point dipole approximation between neighboring islands reveals an interaction scheme which can be mapped to a ferromagnetic interaction in the vertical direction $J_v > 0$ and antiferromagnetic in the horizontal direction $J_h < 0$. The lowest energy state of the array is therefore composed of a staggered arrangement of ferromagnetically aligned chains (see figure 2). The lowest energy state of an asymmetric two-dimensional Ising system is twofold degenerate, in our case corresponding to a ferromagnetic ordering in the vertical direction and an antiferromagnetic ordering in the horizontal direction. Excitations above the ground state occur through the reversal of a macrospin and can be viewed in the form of boundary walls separating the two possible ground states as illustrated in figure 4(c) and the energy state of individual island can be categorized into nine different energy states of varying degeneracy shown in figure 4(d).

Counting the abundances of excitations composed only of independent vertical or horizontal excitations the relative energy scale between the two directions can be attained. The observed probabilities of these excitations decreases exponentially with increasing energy (inset in figure 5) in accordance with a Boltzmann distribution of the states. Determining the ratio of the excitation energies from the inset the energies relating to all energy values of the individual islands can be listed in units of the energy involved with a horizontal excitation $|J_h|$. Within the combined plot (figure 5) the observed abundances decrease exponentially establishing the probability for a macrospin to be in an energy state E to be given by a Boltzmann distribution $\sim \exp(-E/k_B T)$ and that the system can be sufficiently described by a nearest neighbor interaction model.

Identifying the domain walls separating the twofold degenerate ground states of the array facilitates the mapping of the magnetic structure of the system as two ordering states, as illustrated in figure 3. The mapping of
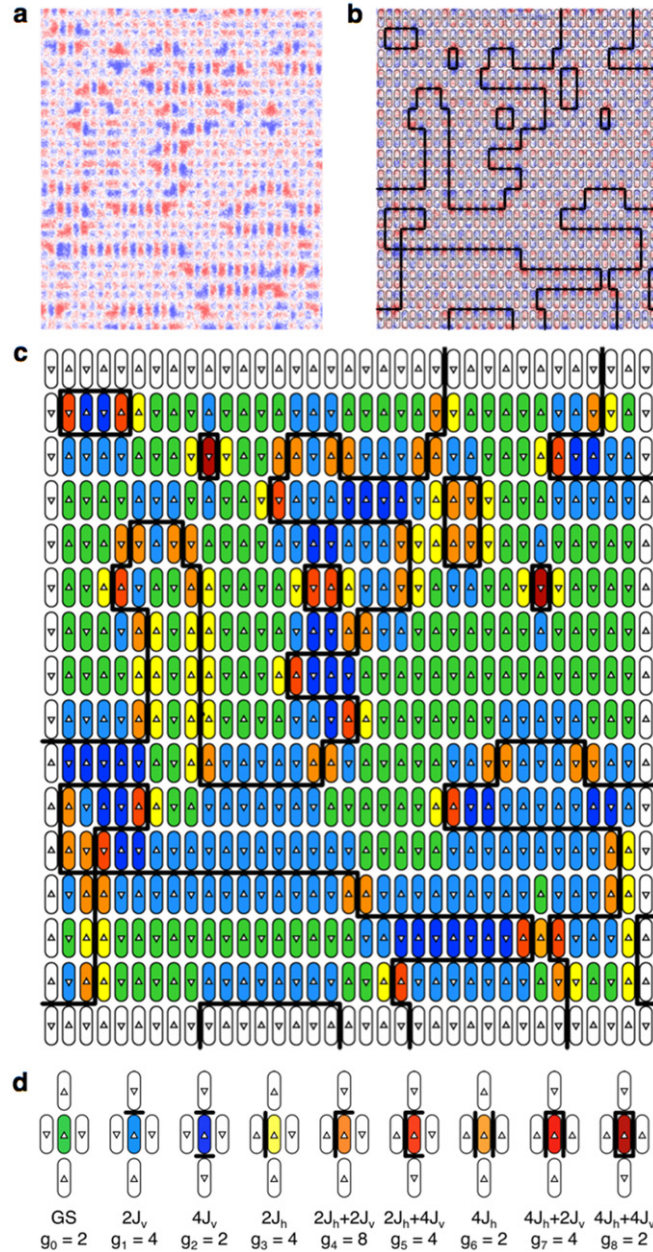
Figure 4. Macrospin arrangements imaged by MFM. Analysis of a part of the MFM images recorded showing a portion of the $N = 10487$ island array for which the direction of the magnetization was determined. The lateral extent of the entire nano-patterned array was 2×2 mm^2, corresponding to a total number of islands of 40 million. (a) Magnetic force microscopy image showing part of the analyzed array. (b) Schematic highlighting of island contours and the excitation boundaries. (c) The energy state of the islands quantified into the nine different possible energy states of individual islands with respect to the orientation of their nearest neighbors shown in (d). The energy states along with their respective degeneracies are listed with respect to the lowest energy ground state assuming that $J_h > J_v$.

these two states onto two domain colors for the entire array is shown in figure 6. Counting the number of islands falling into each of these two domains the order parameter of the array can be obtained. The resulting order parameter for the array, defined by $M = (n_b - n_w)/(n_b + n_w)$, where n_b and n_w correspond to the domain populations of black and white domains, can then be obtained. Truncating the data array to a square shape the array size is reduced to $n = 9828$ out of which $n_b = 5283$ islands fall into the *black* domain while $n_w = 4545$ islands fall into the *white* domain. The resulting value of $M = 0.075 \pm 0.015$ reveals a slightly higher population of the black domains. Although the statistics of this value are limited by the finite number of observed islands in the array it could be indicative of the array being in a state close to, or above T_c, since the lack of global order in the macroscopic arrangement can lead to a finite value of the order parameter. The listed uncertainty of M is determined from the square root of the domain populations, n_w and n_b.

By calculating the pairwise correlation between spins, at a distance **r**, within the experimental array the correlation function for the system, $G(\mathbf{r})$, can be determined. The resulting correlation array is shown in
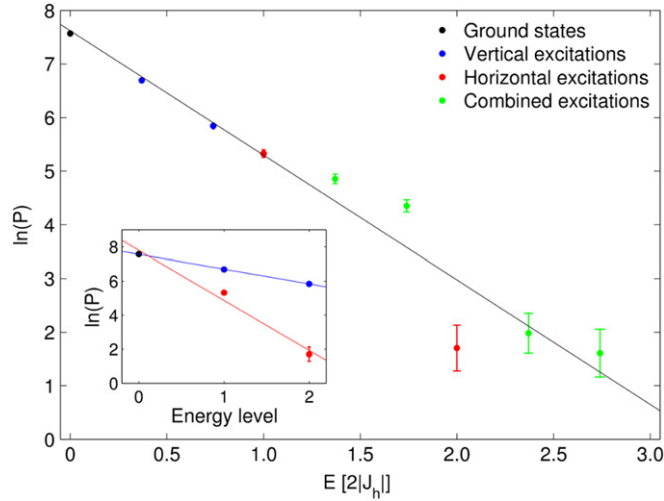
Figure 5. Macrospin energy state statistics. The number of observations of each of the nine energy states illustrated in figure 4(d) divided by their degeneracy. The energy state of a total of 10001 islands was determined. The inset shows the number of observed energy states composed exclusively of either vertical excitations (energy levels $2J_v$ and $4J_v$), blue line, or horizontal excitations (energy levels $2J_h$ and $4J_h$), red line. From the ratio of the slopes the ratio of the energy scale between the vertical and horizontal interaction energies is determined to be $|J_v/J_h| = 0.2943$. Considering this ratio the number of observations of the nine different energy states can be listed as a function of their individual energy in units of $2|J_h|$. The error bars correspond to the square root of the number of observations for each of the energy states.
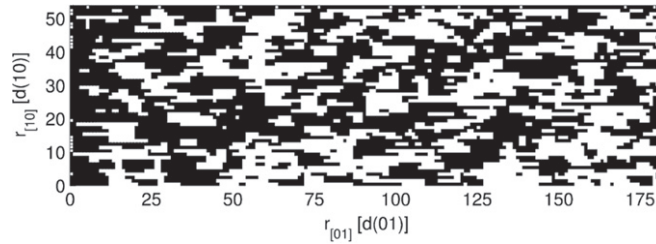

Figure 6. Macrospin array domain configuration. The macrospin configuration of the investigated arrays mapped to black and white domains corresponding to the twofold degenerate ground state of the system.

figure 7. The preference for an antiferromagnetic arrangement of neighboring spins in the [10] direction introduces the possibility of negative values in the correlation and alternating positive and negative values along the [10] direction. Figure 7 therefore shows the absolute value of the pairwise correlation $|G(\mathbf{r})|$ as determined from the array. As can be seen in figure 7 the pairwise correlation follows an exponentially decreasing function as expected for an extended array of Ising like spins at $T > T_c$. Furthermore, the asymmetric nature of the array is revealed in the different values of the correlation lengths along the [10] and [01] directions of the array with $\xi_{[10]} = 2.87$ and $\xi_{[01]} = 1.02$. The correlation length in the [11] direction, $\xi_{[11]} = 0.97$, is revealed to be similar to $\xi_{[01]}$.

The role of the ratio of the interaction strengths on the order parameter and specifically the ordering temperature of the array can be investigated using Onsager's solution, as initially done by Chang [25] or utilizing numerical calculations such as Monte Carlo simulations, see figure 8. In the case of an isotropic system, wherein the interaction strength between neighbors, J, is the same in the two main lattice directions ([01] and [10]), the ordering temperature is given by $T_c = \frac{2J/k_B}{\ln(1 + \sqrt{2})} \approx 2.269J/k_B$. As J_v decreases with respect to J_h the relative T_c of the system also decreases. Figure 8 shows results from Monte Carlo simulations for decreasing values of the ratio $|J_v/J_h|$. The change in T_c corresponds well to what is expected in the two-dimensional Ising model as the probability of observing two parallel spins in the [01] direction decreases. As can be seen in figure 8 the results of numerical simulations correspond well to the analytical solution with small deviations arising from the finite nature of the simulated array.

Assuming a system in a perfectly ordered ground state at $T > 0$ K as the temperature is increased thermal energy is introduced into the system and spins will start to change their directions. The perfect initial order is therefore broken and the system moves towards a thermally disordered state with a reduced order parameter.
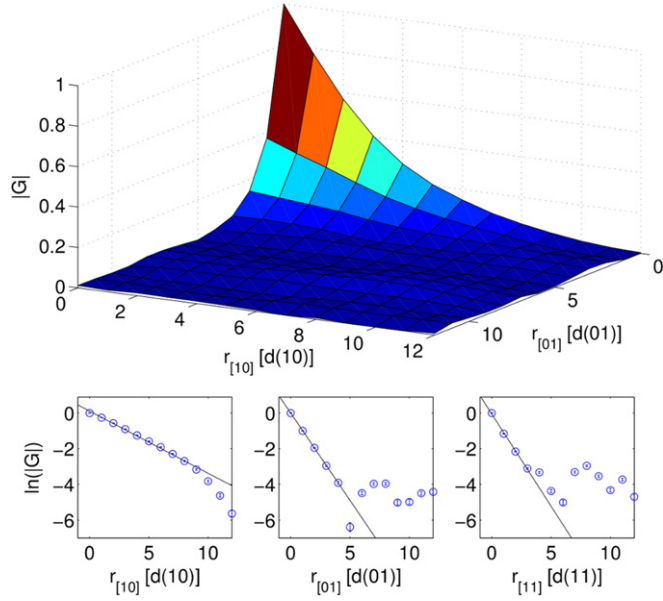
Figure 7. Pairwise correlations *G* for the array. The graph shows the absolute value, |*G*|, for easier mapping of the pairwise correlations for both the ferromagnetic and antiferromagnetic directions. From the slopes the resulting correlation lengths along the different directions is determined to be $\xi_{[10]} = 2.87$, $\xi_{[01]} = 1.02$, and $\xi_{[11]} = 0.97$.

From numerical simulations this transition can, furthermore, be observed through the pairwise correlation $G(\mathbf{r})$ between spins. For the two-dimensional Ising model the correlation decays exponentially with distance towards zero for $T > T_c$ while for $T < T_c$ it decays exponentially towards the square of the spontaneous magnetization per spin [26]. The correlation function can be written as $G(\mathbf{r}) \sim \exp\left(-\frac{\mathbf{r}}{\xi}\right)$ for $T > T_c$, where ξ is the correlation length affected by temperature and the interaction strength between neighboring spins. The inset in figure 8 shows the temperature dependence of ξ for the three major directions of the array, [10], [01], and [11] for the asymmetry ratio $|J_v/J_h| = 0.3$ as determined from Monte Carlo calculations. As $J_h > J_v$ the corresponding correlation length in the [10] direction is larger than in the other directions while the correlation length in the [01] and [11] directions are similar. Considering the results of the Monte Carlo simulations for an interaction ratio of $|J_v/J_h| = 0.3$ one can see that for temperatures larger than T_c the correlation lengths $\xi_{[10]}$ and $\xi_{[01]}$ follow the same trend as the experimental results, i.e. $\xi_{[10]} > \xi_{[01]}$ and $\xi_{[01]} \sim \xi_{[11]}$. In particular at $T = 1.9 J_h/k_B$ the values obtained from the simulations are $\xi_{[10]} = 1.95$, and [01], $\xi_{[01]} = 1.06$, $\xi_{[11]} = 1.08$, similar to the values obtained experimentally.

The interaction strength between neighboring islands was calculated using micromagnetic modeling using rigid spins and assuming a simple dipole model of the macrospins for neighbors up to three lattice constants (see further details in supplementary material). The resulting interaction energies were then used in conjunction with MC simulations to include long-range interactions. However, when including these long-range interactions the correlation lengths were not observed to behave as it is in the experiment, with the [01] direction showing larger correlation lengths than the [10] direction, in contradiction with the experimental observations. This lack of agreement between the micromagnetic analysis and the empirically analyzed array indicates the need for carrying out a detailed analysis of the stray field landscape for the experimental system during the transition from a thermally active state to an arrested state as any modifications to the magnetization within the islands away from a rigid spin state would introduce higher order magnetostatic interactions. The energy landscape is furthermore modified by the arrangement and density of the islands as flux lines are screened by nearer neighbors. Such modifications would affect the energy landscape of the array favouring an increase in energy for nearest neighbors while reducing longer range interactions. From the data we deduce that the magnetic state of the experimental array corresponds to a temperature above the ordering temperature of the system i.e. that the thickness of the islands when the magnetization becomes frozen in is lower than the thickness where the system would undergo the phase transition. However if these thicknesses are similar, effects due to critical slowing down at the phase transition can not be neglected and might affect the final observed state [27]. The good agreement obtained from the nearest neighbor approach applied in the manuscript supports the case that this system is sufficiently described by a nearest neighbor Ising model of dipolar interactions. These results, therefore, indicate that in the arrested state the experimental observations can be described with an effective nearest neighbor Ising model. Hence, long-range dipolar interactions are not needed to model the present
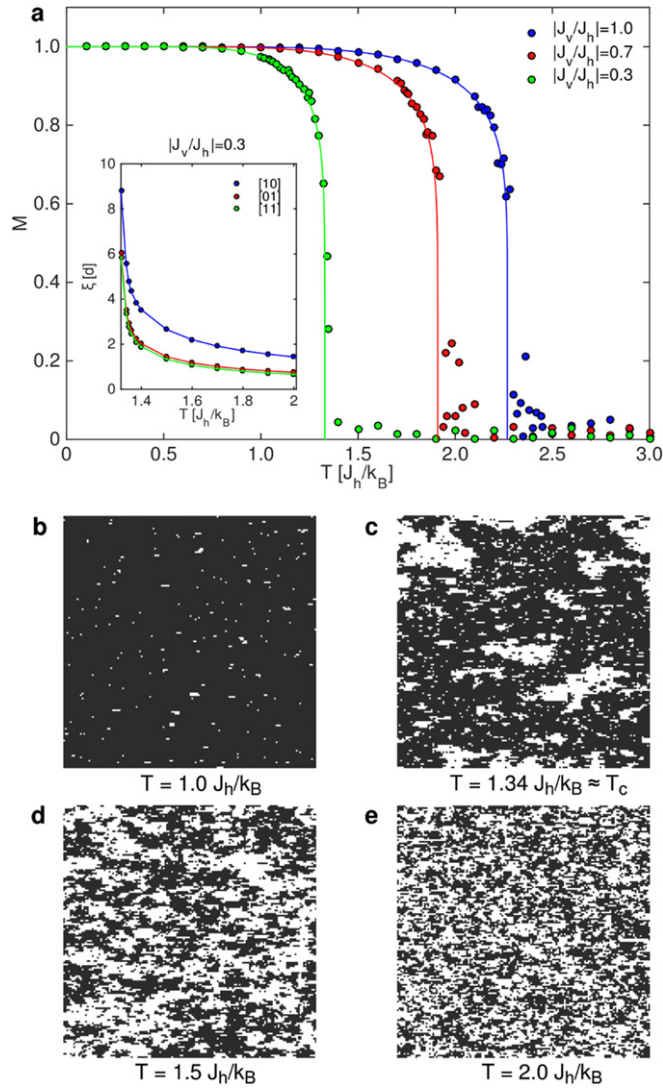
Figure 8. Order parameter versus asymmetry. (a) Results of Monte Carlo simulations showing the order parameter *M* as a function of temperature, in units of J_h/k_B, for different values of $|J_v/J_h|$. Each point in the graph corresponds to an average of several realizations (see information in supplementary material). As the ratio decreases from the symmetric value of the $|J_v/J_h| = 1$ the T_c also decreases. The analytical Onsager solution given by equation (2) (solid lines) fits quite well with the obtained numerical data. The inset shows the correlation length ξ as a function of temperature for the ratio $|J_v/J_h| = 0.3$ for the three major crystallographic directions of the array, [10], [01], and [11]. (b)–(e) Representative snapshots of the numerical simulations at temperatures of $1.0J_h/k_B$, $1.34J_h/k_B$, $1.5J_h/k_B$, and $2.0J_h/k_B$, respectively, for an asymmetry ratio of $|J_v/J_h| = 0.3$. Due to the asymmetry the correlation length in the [10] direction is larger than in the [01] direction stretching out the domains in the [10] direction, similar to what is observed in the experimental data.

system in the arrested stated. However, it should be noted that long-range dipolar interactions cannot be completely excluded if one desires a full description of the system in any non-arrested state.

Further advances in materials science and magnetic imagining techniques will undoubtedly allow us to follow the thermal evolution of a multitude of different artificial spin systems [28] such as artificial spin ice, one- and two-dimensional Ising arrays and different frustrated arrangements [29, 30] as they explore their phase space. Such investigations do not merely offer a direct real space probe of the microstate of thermal systems at a local scale but also a direct determination of the dynamics involved. The possibility of determining directly the state of these systems enables the experimental probing of the effect of external variables such as temperature and applied magnetic field. This introduces the possibility of investigating e.g. the two-dimensional Ising model under applied external field directly for which an analytical solution does not exist.

Acknowledgments

References

[1] Ising E 1925 Beitrag zur theorie des ferromagnetismus *Z. Phys.* **31** 253

[2] Brush Stephen G 1967 History of the Lenz–Ising model *Rev. Mod. Phys.* **39** 883–93

[3] Loth S, Baumann S, Lutz C P, Eigler D M and Heinrich A J 2012 Bistability in atomic-scale antiferromagnets *Science* **335** 196–9

[4] Khalil K S, Sagastegui A, Li Y, Tahir M A, Socolar J E S, Wiley B J and Yellen B B 2012 Binary colloidal structures assembled through Ising interactions *Nat. Commun.* **3** 1798

[5] Zhang S, Gilbert I, Nisoli C, Chern G-W, Erickson M J, O'Brien L, Leighton C, Lammert P E, Crespi V H and Schiffer P 2013 Crystallites of magnetic charges in artificial spin ice *Nature* **500** 553–7

[6] Peierls R 1936 On Ising's model of ferromagnetism *Math. Proc. Camb. Phil. Soc.* **32** 477–81

[7] Onsager L 1944 Crystal statistics: I. A two-dimensional model with an order–disorder transition *Phys. Rev.* **65** 117

[8] Yang C N 1952 The spontaneous magnetization of a two-dimensional Ising model *Phys. Rev.* **85** 808

[9] Imre A, Csaba G, Ji L, Orlov A, Bernstein G H and Porod W 2006 Majority logic gate for magnetic quantum-dot cellular automata *Science* **311** 205–8

[10] Cowburn R P and Welland M E 2000 Room temperature magnetic quantum cellular automata *Science* **287** 1466

[11] Wang R F *et al* 2006 Artificial 'spin ice' in a geometrically frustrated lattice of nanoscale ferromagnetic islands *Nature* **439** 303–6

[12] Nisoli C, Moessner R and Schiffer P 2013 Colloquium: artificial spin ice: designing and imaging magnetic frustration *Rev. Mod. Phys.* **85** 1473–90

[13] Anghinolfi L, Luetkens H, Perron J, Flokstra M G, Sendetskyi O, Suter A, Prokscha T, Derlet P M, Lee S L and Heyderman L J 2015 Thermodynamic phase transitions in a frustrated magnetic metamaterial *Nat. Commun.* **6** 8278

[14] Zhang S *et al* 2012 Perpendicular magnetization and generic realization of the Ising model in artificial spin ice *Phys. Rev. Lett.* **109** 087201

[15] Morgan J P, Stein A, Langridge S and Marrows C H 2011 Thermal ground-state ordering and elementary excitations in artificial magnetic square ice *Nat. Phys.* **7** 75

[16] Mengotti E, Heyderman L J, Fraile Rodríguez A, Nolting F, Hügli R V and Braun H B 2011 Real-space observation of emergent magnetic monopoles and associated Dirac strings in artificial kagome spin ice *Nat. Phys.* **7** 68

[17] Arnalds U B, Farhan A, Chopdekar R V, Kapaklis V, Balan A, Papaioannou E Th, Ahlberg M, Nolting F, Heyderman L J and Hjörvarsson B 2012 Thermalized ground state of artificial kagome spin ice building blocks *Appl. Phys. Lett.* **101** 112404

[18] Kapaklis V, Arnalds U B, Farhan A, Chopdekar R V, Balan A, Scholl A, Heyderman L J and Hjörvarsson B 2014 Thermal fluctuations in artificial spin ice *Nat. Nanotechnology* **9** 514

[19] Daunheimer S A, Petrova O, Tchernyshyov O and Cumings J 2011 Reducing disorder in artificial kagome ice *Phys. Rev. Lett.* **107** 167201

[20] Morgan J P, Akerman J, Stein A, Phatak C, Evans R M L, Langridge S and Christopher C H 2013 Real and effective thermal equilibrium in artificial square spin ices *Phys. Rev.* B **87** 024405

[21] Ahlberg M, Andersson G and Hjörvarsson B 2011 Two-dimensional *XY*-like amorphous $Co_{68}Fe_{24}Zr_8/Al_{70}Zr_{30}$ multilayers *Phys. Rev.* B **83** 224404

[22] Hase T, Raanaei H, Lidbaum H, Sánchez-Hanke C, Wilkins S, Leifer K and Hjörvarsson B 2009 Spin and orbital moment in amorphous $Co_{68}Fe_{24}Zr_8$ layers *Phys. Rev.* B **80** 134402

[23] Arnalds Unnar B, Hase Thomas P A, Papaioannou Evangelos Th, Raanaei H, Abrudan R, Charlton Timothy R, Langridge S and Hjörvarsson B 2012b X-ray resonant magnetic scattering from patterned multilayers *Phys. Rev.* B **86** 064426

[24] Raanaei H, Nguyen H, Andersson G, Lidbaum H, Korelis P, Leifer K and Hjörvarsson B 2009 Imprinting layer specific magnetic anisotropies in amorphous multilayers *J. Appl. Phys.* **106** 023918

[25] Chang C H 1952 The spontaneous magnetization of a two-dimensional rectangular Ising model *Phys. Rev.* **88** 1422

[26] Wu T T 1966 Theory of Toeplitz determinants and the spin correlations of the two-dimensional Ising model: I. *Phys. Rev.* **149** 380

[27] Nisoli C 2012 On thermalization of magnetic nano-arrays at fabrication *New J. Phys.* **14** 035017

[28] Heyderman L J and Stamps R L 2013 Artificial ferroic systems: novel functionality from structure interactions and dynamics *J. Phys. Condens. Matter* **25** 363201

[29] Morrison M J, Nelson T R and Nisoli C 2013 Unhappy vertices in artificial spin ice: new degeneracies from vertex frustration *New J. Phys.* **15** 045009

[30] Gilbert I, Chern G-W, Zhang S, O'Brien L, Fore B, Nisoli C and Schiffer P 2014 Emergent ice rule and magnetic charge screening from vertex frustration in artificial spin ice *Nat. Phys.* **10** 670